Equilibrium and Nonequilibrium Solvation Structure of Hexaammineruthenium (II, III) in Aqueous Solution: Ab Initio RISM-SCF Study†

Hirofumi Sato and Fumio Hirata*

Department of Theoretical Studies, Institute for Molecular Science, and School of Mathematical and Physical Science, The Graduate University for Advanced Studies, Okazaki 444-8585, Japan

Received: July 17, 2001; In Final Form: December 10, 2001

The electronic and solvation structures of the metal complexes in aqueous solutions, $[Ru(NH_3)_6]^{2+}$ and $[Ru(NH_3)_6]^{3+}$, which are key species in electron-transfer reactions, are studied by using RISM−SCF method. We have found that the effective charge on the ruthenium ion does not change so much on the process of oxidation, and the electron is lost mainly from the ligand groups. The electrical potential fluctuations around these complexes are nicely described within a linear-response regime, though some nonlinear effect is observed.

1. Introduction

Electron transfer (ET) reactions have been extensively studied due to essential roles they play in a variety of chemical, physical, and biological processes. Among various types of organometalic complexes, a ruthenium complex has been widely chosen as a model to study the oxidation−reduction chemistry of metalloproteins.[1−3] The ET kinetics has been analyzed in detail for metalloproteins consisting of such as $(Ru(NH_3)_5^{2+})$-a heme protein (cytochrome *c* from horse heart) and $Ru(NH_3)_5(His\text{-}48)^{3+}$-myoglobin, in which the intramolecular electron-transfer proceeds at a significant rate. More fundamental phenomena, ET between the metal complexes in aqueous solution environment, have been investigated by many researchers,[4−10] and the rates and mechanisms of the ET reactions are of great interest from both experimental and theoretical viewpoints.

In the present article, we report a theoretical study for the electronic and solvation structures of $[Ru(NH_3)_6]^{2+}$ and $[Ru(NH_3)_6]^{3+}$ in aqueous solution, which are the fundamental units in the ET processes mentioned above, based on the RISM-SCF method that combines the statistical-mechanics of molecular liquids[11,12] with the ab initio molecular orbital theory.[13−15] It is very perceivable that the electronic structure of a molecule is changed significantly in solution phase. In the RISM-SCF method, the solvent effect on the electronic structure of a solute is taken into account in a mean-field manner, and the simultaneous equations for the solute electronic structure and the solute−solvent correlation functions are solved by minimizing a free energy functional.

The RISM-SCF method has been successful in describing solvation structure and energetics as far as an equilibrium process is concerned. But, in ET recations, the nonequlibrium solvation process, or solvent fluctuations around the redox pair, play a crucial role. Marcus is the first to realize importance of such fluctuations, and to propose the concept of the nonequilibrium free energy profile projected onto a solvent coordinate. The Marcus theory has been validated in numerous experimental and computational ET studies. Recently, Chong and co-workers introduced such solvent fluctuations into the framework of RISM.[16,17] Here, we describe the procedure combining the nonequilibrium aspect of solvation with RISM-SCF method.

The organization of the present paper is as follows. After briefly reviewing the computational procedure, structures of $[Ru(NH_3)_6]^{2+}$ and $[Ru(NH_3)_6]^{3+}$ are discussed in section II. The electronic and solvation structures of those species in aqueous solutions are then described in section III. Section IV concludes the paper.

2. Computational Details

The RISM-SCF/MCSCF theory,[13−15] which we used in the present study, combines two major theoretical elements, the ab initio molecular orbital (MO) theory and the RISM integral equation method. In the thory, electronic structure of a solute molecule in solution and solvent distribution around the solute are solved in a self-consistent manner. More detailed explanation of the theory can be found in the previous reviews and articles.[13−15]

All the MO calculations were performed at the Hartree−Fock (HF) level by using the Dunning-Hay double-ζ basis set with *d*-polarization function on nitrogen ($\alpha = 0.8$). We used the effective core potential and basis set parameters suggested by Stevens el al., in which the 28 inner-shell electrons are replaced with the core potentials.[19] Although the HF-level computations overestimate the Ru−N bond lengths, it is sufficient to describe such molecular properties as geometry changes as pointed out by Broo.[9]

The RISM equations were solved with the hypernetted-chain (HNC) approximation. The SPC-like water model[14] was employed to describe the solvent. The Lennard−Jones parameters of nitrogen and hydrogen in the ruthenium complex were the OPLS parameter set.[20] Unfortunately, the Lennard−Jones parameters for the ruthenium ion were not available in the literatures, we therefore determine the parameters from the MM3 atomic size (σ)[21] and the Mavroynnis−Stephen theory with atomic polarizability.[22] All the parameters are summarized in Table 1. The van der Waals interactions between the atoms in solute and solvent molecules are determined by means of the standard combination rule.[14] The density of water is assumed to be 1.0 g/cm^3 at a temperature of 298.15 K.

The point group symmetry of the hexaammineruthenium is often regarded as the octahedral symmetry (O_h). But the actual symmetry must be lowered due to rotation of the ligand ammonia molecules around the Ru−N bond axis. We examined several geometry optimizations in gas phase under various types

† Part of the special issue "Noboru Mataga Festschrift".

* To whom correspondence should be addressed.

10.1021/jp012760h CCC: $22.00
Published on Web 02/12/2002

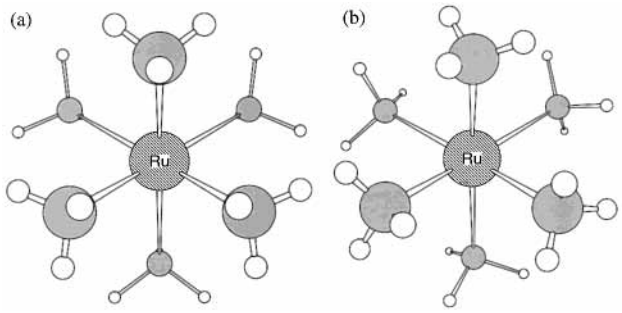

Figure 1. Optimized geometry of hexaammineruthenium ion under the (a) D_{3d} symmetry and (b) D_3 symmetry. A view from the rotational principal axis.

TABLE 1: Lennard−Jones Parameters

atom	σ (Å)	ϵ (kcal mol^{-1})
Hexaammineruthenium (II,III)		
Ru	4.68	0.036
N	3.25	0.170
H	1.07	0.055
Water		
O	3.17	0.155
H	1.00	0.056

TABLE 2: Selected Properties of the Gas Phase Optimized $[Ru(NH_3)_6]^{2+}$ and $[Ru(NH_3)_6]^{3+}$

	$[Ru(NH_3)_6]^{2+}$		$[Ru(NH_3)_6]^{3+}$	
	D_{3d}	D_3	D_{3d}	D_3
Bond Length/Å				
Ru−N	2.277	2.276	2.207	2.208
N−H1[a]	1.008	1.009	1.013	1.014
	(0.0)	(−29.5)	(0.0)	(−29.3)
N−H2[a]	1.008	1.009	1.013	1.013
	(119.8)	(90.2)	(119.3)	(90.6)
N−H3[a]	1.008	1.008	1.013	1.013
	(−119.8)	(−150.2)	(−119.3)	(−149.5)
Mulliken Charge Population[b]/|e|				
Ru	1.2461	1.2229	1.5020	1.4747
N	−1.1295	−1.1329	−1.1407	−1.1456
H1	0.4141	0.4202	0.4567	0.4653
H2	0.4205	0.4193	0.4668	0.4646
H3	0.4205	0.4230	0.4668	0.4699
Energy/au				
	−430.075 34	−430.076 33	−429.535 85	−429.537 31

[a] Values in parentheses are the dihedral angle (principal axis-Ru−N−H) given in deg. [b] The total charge does not give the exact formal charge (+2 or +3) because we present only the four decimal numbers.

of symmetry constraint,[23] and found that the molecular structure with minimum energy possesses the D_3 symmetry (Figure 1 and Table 2). The normal-mode analysis at this geometry did not give any imaginary frequencies, indicating this is in a true local energy-minimum and is very likely to be the global-minimum. As shown in Table 2, electronic structures in the D_{3d} structure do not change so much from that in the D_3, and the energy difference between them is only 0.6 kcal/mol. It is noted that molecular structures (bond length) of the two isomers are very close each other except for rotation of the ammonia group. We thus employed the structure with D_{3d} symmetry in all the computations to reduce computational load, since our main goal in the present study is to clarify physics of the solvation processes associated with a reduction/oxidation reaction in a metal complex.

3. Results and Discussion

3.1. Electronic and Solvation Structure of Hexaammineruthenium. The effective charges are computed by the Mulliken charge population analysis and by the electrostatic potential fitting procedure (ESP). The grid points utilized in the ESP procedure are generated around the solute atoms based on Voronoi polyhedrons[24] of the isocenter spheres with 10 equally spaced radii from 10 to 30 Bohr.

TABLE 3: Effective Atomic Charges in Aqueous Solution and Contributions to the Solvation Free Energy

		effective charges[a]		
		Mulliken	ESP	$\Delta\mu$[b]
$[Ru(NH_3)_6]^{2+}$	Ru	1.2729	2.0035	−169.0
	N	−1.1176	−1.0757	95.5
	H1	0.4047	0.3619	−28.8
	H2	0.4171	0.3566	−28.2
	H3	0.4171	0.3566	−28.2
	total free energy[b]			−107.3
$[Ru(NH_3)_6]^{3+}$	Ru	1.5749	2.1202	−286.0
	N	−1.1305	−1.0500	145.6
	H1	0.4459	0.4061	−51.8
	H2	0.4610	0.3952	−49.9
	H3	0.4610	0.3952	−49.9
	total free energy[b]			−322.7

[a] See the footnote in Table 2. [b] All the energies are given in kcal mol^{-1}.

The solvation free energy ($\Delta\mu$) can be decomposed and assigned to contribution from each atom (α) in the solute, because $\Delta\mu$ is "formally" expressed as a sum of the site−site contributions[25]

$$\Delta\mu = \sum_{\alpha} \Delta\mu_{\alpha} \tag{1}$$

It is noted that $\Delta\mu_{\alpha}$ is not the same as the solvation free energy of an atom α isolated in the solvent because the correlation functions in $\Delta\mu_{\alpha}$ also depend on other atoms in the solute.

In Table 3, the results for effective charges and solvation free energies are listed. One can readily see that the effective charges evaluated from the two methods are slightly different: the charges on ruthenium atom by ESP are much greater than those by the Mulliken analysis, but the trend of their change upon the ionization (+2 → +3) is quite similar except for the nitrogen atoms. The effective charges on the ruthenium and hydrogen atoms are positive and become larger upon the ionization in the both methods, whereas the charge on nitrogen atoms changes in the opposite directions by the two methods. It is not trivial to judge which method represents the effective charges properly because each method reflects different characteristics of the electronic structure: the Mulliken analysis represents the distribution of electron density, whereas the ESP charge is determined so as to reproduce the electrostatic potential near the solute molecule. In any case, it is important to note that the change of charges on the ruthenium ion upon the oxidation is not so large, and the electron deffect is considerably delocalized over the whole complex.

As shown in Table 3, the greatest contribution to the solvation free energy comes from the ruthenium ion, although the ion is supposed to be completely embedded in the surrounding ammonia ligands and lacks the direct contact with solvent molecules. The large and negative free energy of solvation is obviously attributed to the strong electrostatic interaction due to the charge on the ion. The contribution from the hydrogen atoms is another source of the solvation free energy. It should be mentioned that there are eighteen hydrogen atoms in this metal complex and the total amount of the solvation free energy originated in these hydrogens is much greater than that in the ruthenium ion. The positively large free energy assigned to the

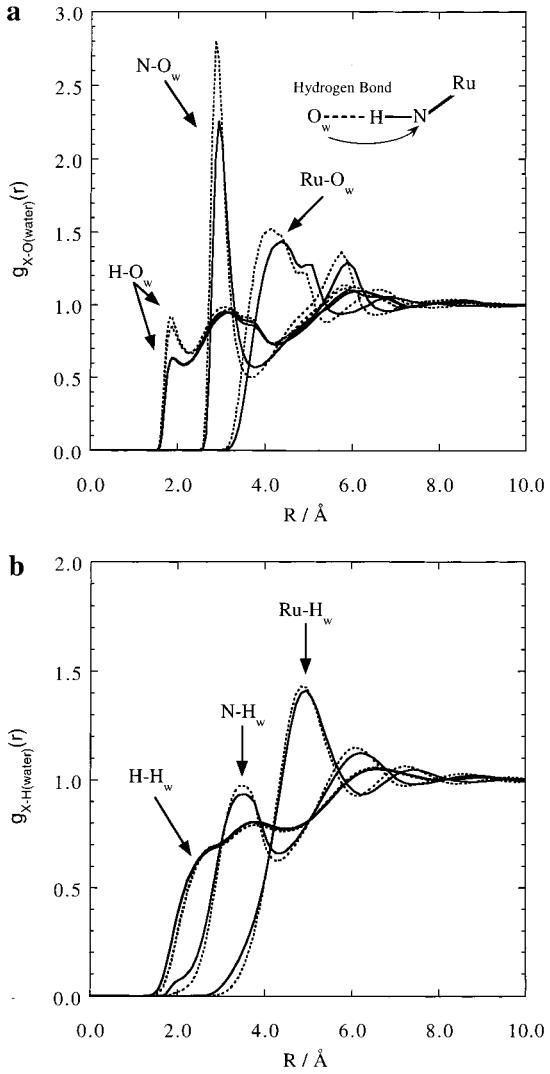

Figure 2. (a) Pair correlation function between the ruthenium complex and water oxygen (O_w). Solid lines for $[Ru(NH_3)_6]^{2+}$ and dashed lines for $[Ru(NH_3)_6]^{3+}$. (b) Pair correlation function between the ruthenium complex and water hydrogen (H_w). Solid lines for $[Ru(NH_3)_6]^{2+}$ and dashed lines for $[Ru(NH_3)_6]^{3+}$.

nitrogen atoms can be explained in terms of repulsive interaction between the nitrogen and oxygen atoms. Therefore, the stabilization of $[Ru(NH_3)_6]^{2+}$ or $[Ru(NH_3)_6]^{3+}$ in energy can be understood as the sum of the contribution from the great charge on the central ruthenium and from the eighteen hydrogen bondings.

All the site−site pair correlation functions (PCF) between the two metal complexes ($[Ru(NH_3)_6]^{2+}$ and $[Ru(NH_3)_6]^{3+}$) and solvent water molecules are shown in Figure 2. The most important in these figures is the peak around 1.9 Å in the H−O_w (oxygen atom in the solvent water) PCF (Figure 2(a)). By simple geometrical considerations, this can be assigned to the hydrogen bond between the hydrogen atom in ammonia ligand and the solvent oxygen. The conspicuous peak around 3.0 Å in the N−O_w PCF is another evidence of the strong hydrogen bond as depicted in the figure. Although there are two types of hydrogen atoms in the ammonia ligands under the D_{3d} symmetry, which correspond to H1 and H2 in Table 2 (H2 and H3 are the equivalent), their PCF are almost identical, especially in $[Ru(NH_3)_6]^{2+}$. An interesting feature in the figure is that all the peak positions in PCF of $[Ru(NH_3)_6]^{2+}$ (solid line in the figure) and those in $[Ru(NH_3)_6]^{3+}$ (dashed line) is very close each other and only the peak height is slightly greater in $[Ru(NH_3)_6]^{3+}$ than that in $[Ru(NH_3)_6]^{2+}$. This indicates that the solvation structures around the $[Ru(NH_3)_6]^{2+}$ and $[Ru(NH_3)_6]^{3+}$ are very similar, which is due, probably, to saturation of the electrostatic effect.

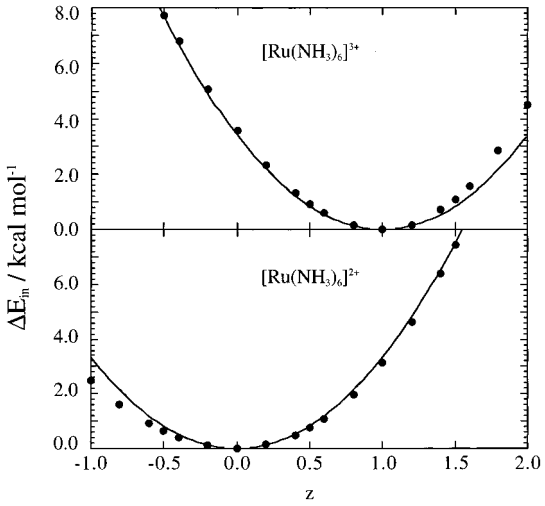

Figure 3. Potential energy change along the fraction coordinate of z for $[Ru(NH_3)_6]^{2+}$ (lower panel) and $[Ru(NH_3)_6]^{3+}$ (upper panel). Solid lines represent fitting curves with harmonic approximation.

3.2. Equilibrium and Nonequilibrium Processes of Solvation. It is known that the electron-transfer process in outer sphere mechanism is governed by the intramolecular symmetric stretching along the metal−ligand bond ("breathing mode") and by the solvent fluctuation around the solute. In the following section, we consider a redox process of the complex in terms of these two coordinates.

Prior to describing the process in solution, we first consider the redox process in gas phase. Because the molecular structure of the ruthenium complex must change from the $[Ru(NH_3)_6]^{2+}$ structure (before oxidation) to the $[Ru(NH_3)_6]^{3+}$ (after oxidation) both in the optimized structures, it is reasonable to model the geometrical change by a linear interpolation of these structures

$$\mathbf{x} = (1 - z)\mathbf{x}_{2+} + z\mathbf{x}_{3+} = \mathbf{x}_{2+} + z(\mathbf{x}_{3+} - \mathbf{x}_{2+}) = \mathbf{x}_{2+} + z\Delta\mathbf{x} \tag{2}$$

where $\mathbf{x}$ expresses a transient structure at the mixing of z, $\mathbf{x}_{2+}$ and $\mathbf{x}_{3+}$ are the optimized structure of di- and trivalent cations, respectively. The potential energy profile along this coordinate z are shown in Figure 3. Their curvatures are satisfactorily approximated with quadratic functions, especially near the two optimized structures ($0 \le z \le 1$). The expansion by the normal modes at the two cations indicates that the motion ($\Delta\mathbf{x}$) consists of purely one mode (about 98% for the both sets of the normal modes) around 400 cm^{-1}, which is assigned to the symmetric metal−ligand stretching.

A diabatic free energy profile in polar solvent can be realized within the framework of the RISM theory by Chong's method,[16,17] in which the hypothetical charge distribution is introduced. Although the method was originally developed for the two reacting particles (donor and acceptor), extension to a polyatomic system is straightforward. Let $\mathbf{q}_{+2}$ and $\mathbf{q}_{+3}$ denote the charge set of di- and trivalent cations obtained by RISM-SCF procedure, respectively

$$^t\mathbf{q}_{+2} = (q^1_{+2}, q^2_{+2}, q^3_{+2}, \cdots q^N_{+2})$$
$$^t\mathbf{q}_{+3} = (q^1_{+3}, q^2_{+3}, q^3_{+3}, \cdots q^N_{+3}) \tag{3}$$

where N is the total number of atoms (sites) in the reacting species. A hypothetical charge distribution, as the function of fraction s, is introduced as follows

$$\mathbf{q} = (1 - s)\mathbf{q}_{2+} + s\mathbf{q}_{3+} \tag{4}$$

The free energy change from the dication ($\Delta\mu_{2+}$ with $\mathbf{q}_{+2}$) to a state with the hypothetical charges ($\Delta\mu_s$ with $\mathbf{q}$) is then given by

$$\Delta\mu_s - \Delta\mu_{2+} = -\frac{1}{\beta}\ln\langle e^{-\beta s\Delta H}\rangle \tag{5}$$

$s\Delta H$ is the difference of the Hamiltonian of the two states, H_s and H_{2+}, and is usually expressed as change of the electrostatic part

$$s\Delta H = s\sum_{i,j}\frac{(q^i_{3+} - q^i_{2+})q^j_{\text{solvent}}}{|\mathbf{r}_i - \mathbf{r}_j|} = s\sum_{i,j}\frac{\Delta q^i q^j_{solvent}}{|\mathbf{r}_i - \mathbf{r}_j|} \tag{6}$$

where

$$\Delta\mathbf{q} = \mathbf{q}_{+3} - \mathbf{q}_{+2} \tag{7}$$

and $\mathbf{r}_i$ and $\mathbf{r}_j$ are the position of solute sites (i) and solvent sites (j), respectively. q_{solvent} is the fixed charge assigned to the solvent site. Equation 5 can be rewritten in the cumulative expansion[16,17]

$$\Delta\mu_s - \Delta\mu_{2+} = \frac{1}{\beta}\sum_{n=1}^{\infty}\frac{(-s\beta)^n}{n!}\langle(\Delta H)^n\rangle_{2+,c}$$

$$= s\langle\Delta H\rangle_{2+,c} - \frac{\beta}{2}s^2\langle(\Delta H)^2\rangle_{2+,c} + \frac{\beta^2}{6}s^3\langle(\Delta H)^3\rangle_{2+,c} + \mathcal{O}(s^4)$$

Because there is a relation in s-expansion for $\langle\Delta H\rangle_s$, (see the appendix in ref 17 for detail)

$$\langle\Delta H\rangle_s = \langle\Delta H\rangle_{2+,c} - \beta s\langle(\Delta H)^2\rangle_{2+,c} + \frac{\beta^2}{2}s^2\langle(\Delta H)^3\rangle_{2+,c} + \mathcal{O}(s^3) \tag{8}$$

The free energy difference between the two states is given by

$$\Delta\mu_s - \Delta\mu_{2+} = s\langle\Delta H\rangle_s + \frac{\beta}{2}s^2\langle(\Delta H)^2\rangle_{2+,c} - \frac{\beta^2}{3}s^3\langle(\Delta H)^3\rangle_{2+,c} + \mathcal{O}(s^4) \tag{9}$$

where $\mathcal{O}(s^n)$ denotes the higher order terms. $\langle\Delta H\rangle_s$ is widely used as a reaction coordinate and can be computed with electrostatic potential on the solute site $\mathbf{V}_s$ whose component is

$$(\mathbf{V}_s)_i = \rho\sum_j q^j_{\text{solvent}}\int dr\, 4\pi r^2\frac{g^s_{ij}(r)}{r} \tag{10}$$

and

$$\langle\Delta H\rangle_s = \mathbf{V}_s\cdot\Delta\mathbf{q} \tag{11}$$

Note that $\mathbf{V}_s$ is a function of the fraction s because $g^s_{ij}(r)$ is the PCF calculated with the hypothetical charge distribution ($\mathbf{q}$). Figure 4 shows the reaction coordinate $\langle\Delta H\rangle_s$ as well as the averaged potential energy (U) and solvation free energy for the hypothetical state ($\Delta\mu_s$). The $\langle\Delta H\rangle_s$ shows linear dependency on s.

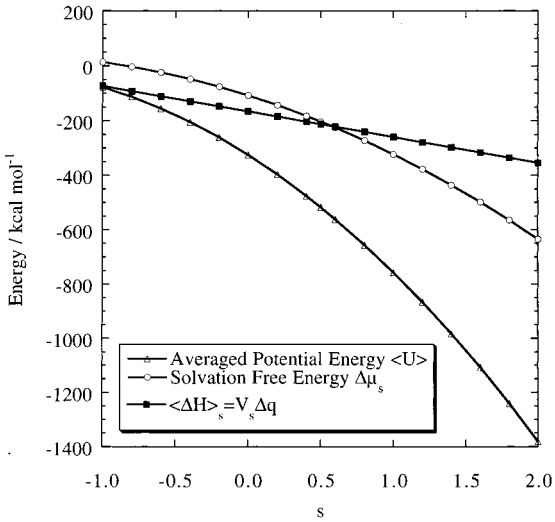

Figure 4. Reaction coordinate ($\mathbf{V}_s\Delta\mathbf{q}$), averaged interaction energy ($\langle U\rangle_s$) and solvation free energy ($\Delta\mu_s$) as functions of the fraction of s. Solid lines represent fitting curves with harmonic approximation.

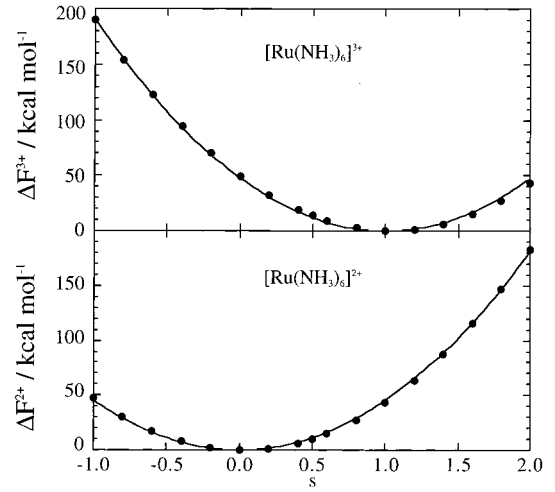

Figure 5. Free energy profile along the fraction s for $[Ru(NH_3)_6]^{2+}$ (lower panel) and $[Ru(NH_3)_6]^{3+}$ (upper panel). Solid lines represent fitting curves with harmonic approximation.

Then, the free energy profile (ΔF^{2+}) around the actual solute charge distribution ($\mathbf{q}_{+2}$) is given by

$$\Delta F^{2+}(s) = \Delta\mu_s - \Delta\mu_{2+} - s\mathbf{V}_s\cdot\Delta\mathbf{q} \tag{12}$$

The curve for the product state ($[Ru(NH_3)_6]^{3+}$) can be obtained by the similar procedure

$$\Delta F^{3+}(s) = \Delta\mu_s - \Delta\mu_{3+} - (s-1)\mathbf{V}_s\cdot\Delta\mathbf{q} \tag{13}$$

The diabatic free energy profile obtained by the method is plotted in Figures 5 and 6. In the present study, the fraction of the electronic charge transfer (s) and that of the geometrical change (z) are simultaneously varied along the electron transfer process. The most notable feature of the figures is that it is essentially parabolic with respect to the reaction coordinate. The electron-transfer reaction between the ruthenium complex

$$[Ru(NH_3)_6]^{2+} + [Ru(NH_3)_6]^{3+} \rightleftharpoons [Ru(NH_3)_6]^{3+} + [Ru(NH_3)_6]^{2+}$$

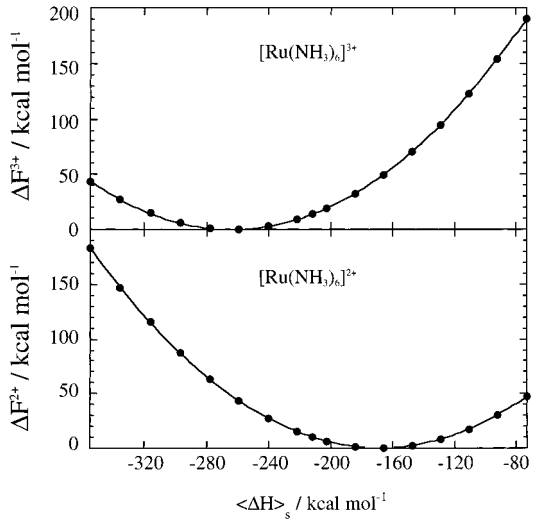

Figure 6. Free energy profile along the reaction coordinate ($\mathbf{V}_s\Delta\mathbf{q}$) for $[Ru(NH_3)_6]^{2+}$ (lower panel) and $[Ru(NH_3)_6]^{3+}$ (upper panel). Solid lines represent fitting curves with harmonic approximation.

is a symmetric reaction. The activation free energy of the present system ($\Delta G^{\ddagger}$) can be estimated with the relation

$$\Delta G^{\ddagger} \approx \Delta F^{2+}\left(\frac{1}{2}\right) + \Delta F^{3+}\left(\frac{1}{2}\right)$$

which gives 24 kcal mol^{-1}. Unfortunately, experimental data directly corresponding to the theoretical result is not available at the moment. Here, we just refer to the experimental value, ~14 kcal mol^{-1},[7] obtained for the same metal complex in the different solvent condition (involving CF_3SO_3H and counterions). The present model treats these metal complexes in pure aqueous solution and the screening from counterions as well as CF_3SO_3H is completely disregarded. The screening effect in general weakens the ion−ion interactions, in this case, repulsive ones, and the effect very likely lowers $\Delta G^{\ddagger}$. In principle, it is possible to evaluate the magnitude of the screening by taking all the counterions into account. However, such calculations that involve averaging over the orientations and estimation of the orbital overlaps between the complexes, are very time demanding and impractical by any means. This is obviously out of scope of the present paper.

4. Conclusions

We have reported a study of solvation and electronic structure for the two metal complexes, $[Ru(NH_3)_6]^{2+}$ and $[Ru(NH_3)_6]^{3+}$, in aqueous solutions, carried out by the ab initio RISM-SCF method in which solvent effect is treated in molecular level. The solvation free energy profile is computed as a function of the charge fraction that concerned with the electronic structure of a solute molecule. As far as we know, this is the first to study a nonequilibrium energy profile by means of the RISM-SCF method.

The electronic structures of $[Ru(NH_3)_6]^{2+}$ and $[Ru(NH_3)_6]^{3+}$ in aqueous solutions are characterized by the localized charge on the central ion. We found that the ESP charge on the metal, an effective charge that surrounding solvent molecules look upon, does not change much upon the oxidation process, and the electron is lost mainly from the ligand groups. We have computed the "Marcus parabola" along the electrical fluctuation of solvent from the first principle.

The method proposed in the present paper, the combination of RISM-SCF and the method to evaluate the electrical fluctuation of solvent, is promising to tackle various issues in physical chemistry, understanding chemical reactions in solution, prediction of spectral bandwidth, and so on. However, to improve the agreement with the experimental measurements, screening from counterions should be taken into account. The choice of the reaction coordinate ($\langle\Delta H\rangle_s$ in the present study) is another key to contact with experimental data. The research in this direction is currently underway in our group.

Acknowledgment. This research was supported by the Grant-in Aid for Scientific Research on Priority Areas 'Molecular Physical Chemistry' (403-11166276), Grant-in Aid for Encouragement of Young Scientists (12740329), and from the Japanese Ministry of Education, Science, Sports and Culture (MONBU SHO).

References and Notes

(1) Creutz, C.; Sutin, N. *J. Biol. Chem.* **1974**, *21*, 6788; Chou, M.; Creutz, C.; Sutin, N. *J. Am. Chem. Soc.* **1977**, *99*, 5615; Sutin, N. *Acc. Chem. Res.* **1982**, *15*, 275.

(2) Ewall, R. X.; Bennett, L. E. *J. Am. Chem. Soc*. **1974**, *96*, 940.

(3) Winkler, J. R.; Nocera, D. G.; Yacom, K. M.; Bordignon, E.; Gray, H. B. *J. Am. Chem. Soc*. **1982**, *104*, 5798; Nocera, D. G.; Winkler, J. R.; Yacom, K. M.; Bordignon, E.; Gray, H. B. *J. Am. Chem. Soc*. **1984**, *106*, 5145; Axup, A. W.; Albin, M.; Mayo, S. L.; Crutchley, R. J.; Gray, H. B. *J. Am. Chem. Soc*. **1988**, *110*, 435.

(4) Endicott, J. F.; Taube, H. *J. Am. Chem. Soc*. **1962**, *84*, 4984; *J. Am. Chem. Soc*. **1964**, *86*, 1686; *Inorg. Chem*. **1965**, *4*, 437.

(5) Stynes, H. C.; Ibers, J. A. *Inorg. Chem*. **1971**, *10*, 2304.

(6) Daul, C.; Goursot, A. *Inorg. Chem*. **1985**, *24*, 3554.

(7) Lavallee, D. K.; Lavallee, C.; Sullivan, J. C.; Deutsch, E. *Inorg. Chem*. **1973**, *12*, 570.

(8) Ondrechen, M. J.; Ratner, M. A.; Ellis, D. E. *J. Am. Chem. Soc*. **1981**, *103*, 1656.

(9) Broo, A. *Int. J. Quantum Chem*. **1996**, *30*, 1331.

(10) Newton, M. D. *Int. J. Quantum Chem*. **1980**, *14*, 363; Logan, J.; Newton, M. D.; Noell, J. O. *Int. J. Quantum Chem*. **1984**, *18*, 213; Newton, M. D. *J. Phys. Chem*. **1986**, *90*, 3734.

(11) Chandler, D.; Andersen, H. C. *J. Chem. Phys*. **1972**, *57*, 1930.

(12) Hirata, F.; Rossky, P. J. *Chem. Phys. Lett*. **1981**, *83*, 329; Hirata, F.; Pettitt, B. M.; Rossky, P. J. *J. Chem. Phys*. **1982**, *77*, 509; Hirata, F.; Rossky, P. J.; Pettitt, B. M. *J. Chem. Phys*. **1983**, *78*, 4133.

(13) Hirata, F.; Sato, H.; Ten-no, S.; Kato, S. *Combined Quantum Mechanical and Molecular Mechanical Methods*; ACS Symposium Series 712; American Chemical Society: Washington, DC, 1998; p 188; Hirata, F.; Sato, H.; Ten-no, S.; Kato, S. The RISM-SCF/MCSCF Approach for the Chemical Processes in Solutions. In *Computational Biochemistry and Biophysics*; Becker, M. O., MacKerell, D. A., Jr., Roux, B., Watanabe, M., Eds.; Marcel Dekker Inc.: New York, 2001; Chapter 19, pp 417−439.

(14) Ten-no, S.; Hirata, F.; Kato, S. *J. Chem. Phys*. **1994**, *100*, 7443.

(15) Sato, H.; Hirata, F.; Kato, S. *J. Chem. Phys*. **1996**, *105*, 1546.

(16) Chong, S.-H.; Miura, S.; Basu, G.; Hirata, F. *J. Phys. Chem*. **1995**, *99*, 10526; Chong, S.-H.; Hirata, F. *Mol. Simulation* **1996**, *16*, 3; Chong, S.-H.; Hirata, F. *Chem. Phys. Lett*. **1988**, *293*, 119; Akiyama, R.; Kinoshita, M.; Hirata, F. *Chem. Phys. Lett*. **1999**, *305*, 251.

(17) Chong, S.-H.; Hirata, F. *J. Chem. Phys*. **1997**, *106*, 5225.

(18) Dunning, T. H., Jr.; Hay, P. J. In *Methods of Electronic Structure Theory*; Shaefer, H. F., III., Ed.; Plenum Press: New York, 1977; pp 1−27.

(19) Stevens, W. J.; Basch, H.; Krauss, M.; Jasien, P. *Can. J. Chem*. **1992**, *70*, 612.

(20) Jorgensen, W. L.; Briggs, J. M.; Contreras, M. L. *J. Phys. Chem*. **1990**, *94*, 1683.

(21) Allinger, N. L.; Zhou, X.; Bergsma, J. *J. Mol. Struct. (THEOCHEM)* **1994**, *312*, 69.

(22) Sato, H.; Hirata, F. *J. Am. Chem. Soc*. **1999**, *121*, 3460.

(23) We have examined geometry optimization under the restriction of D_3 symmetry for one isomer, D_{3d} for two and C_{2v} for four. All the energies in these isomers are very close to each other: maximum is +0.17 (one of the C_{2v}) and minimum is −0.62 kcal/mol (one of the D_3, shown in Table 2) compared to the D_{3d} isomer (shown in Table 2), respectively.

(24) Naka, K.; Sato, H.; Morita, A.; Hirata, F.; Kato, S. *Theor. Chem. Acc*. **1999**, *102*, 165.

(25) Sato, H.; Hirata, F. *J. Mol. Struct. (THEOCHEM)* **1999**, *113*, 461−462.